Available online at www.sciencedirect.com
SCIENCE DIRECT®
ELSEVIER
Journal of Electron Spectroscopy and Related Phenomena 137–140 (2004) 705–711
JOURNAL OF ELECTRON SPECTROSCOPY and Related Phenomena
www.elsevier.com/locate/elspec

Quasi-monochromatic parallel radiography utilizing a computed radiography system

E. Sato[a,*], Y. Hayasi[a], R. Germer[b], E. Tanaka[c], H. Mori[d], T. Kawai[e], T. Ichimaru[f], S. Sato[g], K. Takayama[h], H. Ido[i]

[a] *Department of Physics, Iwate Medical University, Morioka 020-0015, Japan*
[b] *ITP, FHTW FB1 and TU-Berlin, D 12249 Berlin, Germany*
[c] *Department of Nutritional Science, Faculty of Applied Bio-science, Tokyo University of Agriculture, Setagayaku 156-8502, Japan*
[d] *Department of Cardiac Physiology, National Cardiovascular Center Research Institute, Osaka 565-8565, Japan*
[e] *Electron Tube Division #2, Hamamatsu Photonics Inc., Iwata-gun 438-0193, Japan*
[f] *Department of Radiological Technology, School of Health Sciences, Hirosaki University, Hirosaki 036-8564, Japan*
[g] *Department of Microbiology, School of Medicine, Iwate Medical University, Morioka 020-8505, Japan*
[h] *Shock Wave Research Center, Institute of Fluid Science, Tohoku University, Sendai 980-8577, Japan*
[i] *Department of Applied Physics and Informatics, Faculty of Engineering, Tohoku Gakuin University, Tagajo 985-8537, Japan*

Available online 21 March 2004

Abstract

A fundamental study on quasi-monochromatic parallel radiography using a polycapillary plate and a copper-target X-ray tube is described. The X-ray generator consists of a negative high-voltage power supply, a filament (hot cathode) power supply, and an X-ray tube. The negative high-voltage is applied to the cathode electrode, and the anode electrode is connected to the ground. In this experiment, the tube voltage was regulated from12–25 kV, and the tube current was regulated within 3.0 mA by the filament temperature. The exposure time was controlled in order to obtain optimum X-ray intensity, and the maximum focal spot dimensions were approximately 2 mm × 1.5 mm. The polycapillary plate was J5022-21 (Hamamatsu Photonics Inc.), and the plate thickness was 1.0 mm. The outer, effective, and hole diameters were 87 mm, 77 mm, and 25 μm, respectively. Quasi-monochromatic X-rays were produced using a 10 μm-thick copper filter, and these rays were formed into parallel beams by the polycapillary, and the radiogram was taken using a computed radiography system utilizing imaging plates. In the measurement of image resolution, the resolution fell according to increases in the distance between the chart and imaging plate using a polycapillary. We could observe a 50 μm tungsten wire clearly, and fine blood vessels of approximately 100 μm were visible in angiography.

Keywords: Parallel radiography; Quasi-monochromatic X-ray; Characteristic X-ray; X-ray lens; Polycapillary plate

1. Introduction

Thus far, we have developed several different soft flash X-ray generators [1–8] in order to perform soft radiographies with biomedical applications. In particular, plasma flash X-ray generators [9–11] are very useful to produce fairly high-dose-rate monochromatic X-rays as compared with a synchrotron. When a weakly ionized linear plasma formed using a rod target evaporation, irradiation of quite intense and sharp characteristic X-rays from the plasma axial direction was confirmed.

Monochromatic parallel radiography using synchrotrons plays important roles in microangiography [12] and X-ray phase imaging, [13–15] and further applications have long been wished for. In view of this situation, several different X-ray lenses have been developed [16,17], and a polycapillary plate [18–20] has been shown to be useful to realize a low-priced X-ray system and to perform parallel radiography. Therefore, we performed parallel radiography using a tungsten-target X-ray tube [19] and an X-ray film, and an image resolution of approximately 50 μm or less was obtained.

The tungsten target produced L-series characteristic and bremsstrahlung X-rays with tube voltages of 20–30 kV, and these rays were formed into parallel beams to perform radiography. Thereafter, K-series characteristic X-rays could

* Corresponding author.
E-mail address: dresato@iwate-med.ac.jp (E. Sato).

0368-2048/$ – see front matter © 2004 Elsevier B.V. All rights reserved.
doi:10.1016/j.elspec.2004.02.008

be employed for quasi-monochromatic and monochromatic radiographies using filters. In these cases, the photon energies of characteristic X-rays were determined by the target element.

In this research, we performed preliminary study on quasi-monochromatic parallel radiography utilizing a polycapillary plate, a Computed Radiography (CR) system [21], and a copper-target radiation tube in order to create a new X-ray system to be used instead of the synchrotron.

2. Experimental set-up

Fig. 1 shows the circuit diagram of the X-ray generator, which consists of a negative high-voltage power supply, a filament (hot cathode) power supply, and a copper-target X-ray tube. The negative high-voltage is applied to the cathode electrode, and the anode (target) is connected to the ground. In this experiment, the tube voltage was regulated from 15–25 kV, and the tube current was regulated by the filament temperature and ranged from 1.0–3.0 mA. The exposure time was controlled in order to obtain optimum X-ray intensity.

The experimental set-up for performing parallel radiography is shown in Fig. 2. Quasi-monochromatic X-rays are produced using a 10 μm-thick copper filter, and these rays are formed into parallel beams by a polycapillary plate. The polycapillary is J5022-21 (Hamamatsu Photonics Inc.), and the thickness and the hole diameter of the polycapillary are

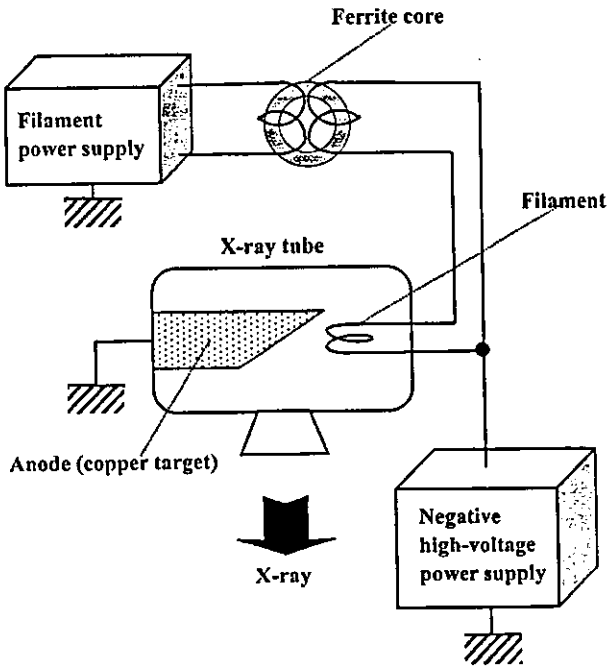

Fig. 1. Circuit diagram of the X-ray generator. Because the negative high voltage is applied to the cathode electrode, the tube voltage is −1 times the cathode voltage. The X-ray tube employs a 0.5 mm-thick beryllium window in order to produce soft X-rays effectively.

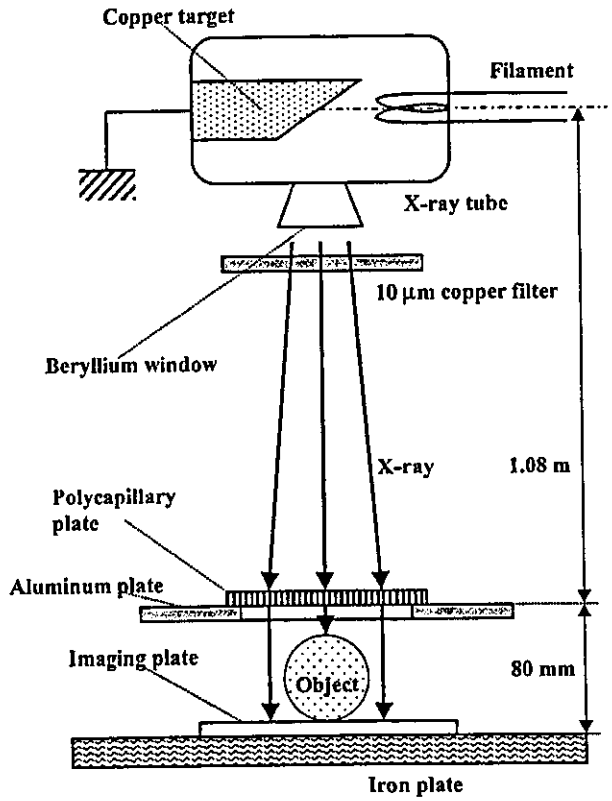

Fig. 2. Experimental set-up for parallel radiography utilizing a polycapillary plate and a CR system. Quasi-monochromatic X-rays are formed into parallel beam by a polycapillary, and the image is taken by a CR system.

1.0 mm and 25 μm, respectively (Fig. 3). Radiography was performed by a CR system (Konica Regius 150) utilizing imaging plates.

The distance between the X-ray source and the polycapillary was 1.08 m, and the polycapillary plate was placed on the aluminum plate, and the distance between the aluminum and imaging plates was regulated by the height of polymethyl methacrylate (PMMA) spacers of 30 mm in height.

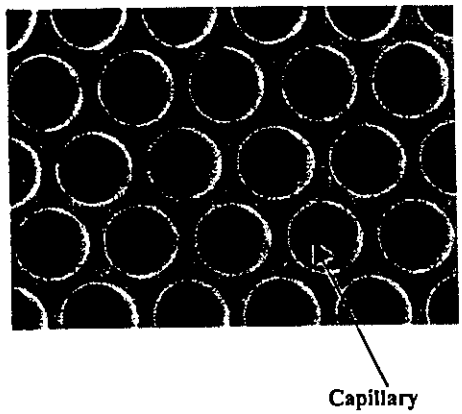

Fig. 3. Magnification of a polycapillary plate with a thickness of 1.0 mm and a hole diameter of 25 μm, respectively.

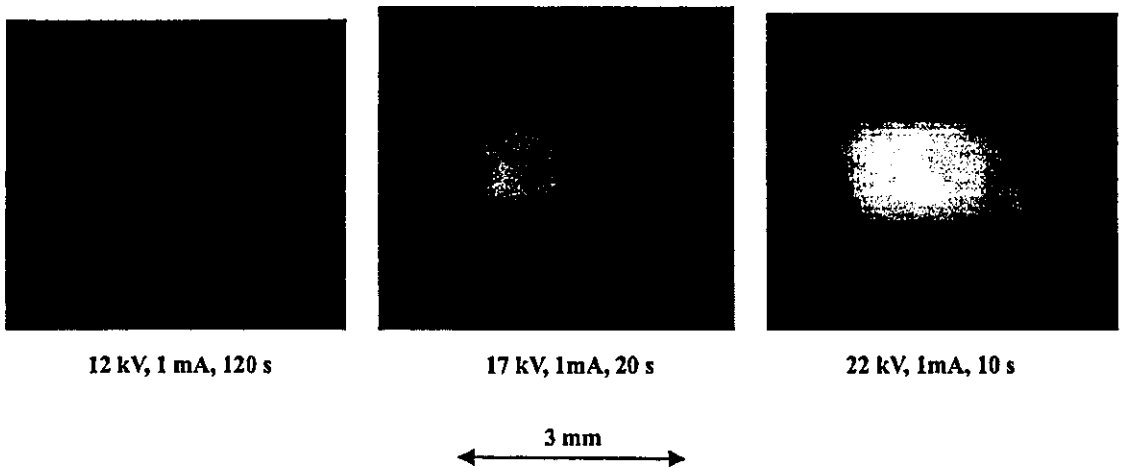

Fig. 4. Images of the X-ray source measured by a 50 μm-diameter pinhole with changes in the tube voltage.

3. Characteristics

3.1. Focal spot

In order to measure images of the X-ray source, we employed a pinhole camera with a hole diameter of 50 μm (Fig. 4). When the tube voltage was increased, the spot intensity increased, and spot dimensions increased slightly and had values of approximately 2 mm × 1.5 mm.

3.2. X-ray spectra

X-ray spectra from the copper-target tube were measured by a transmission-type spectrometer (Fig. 5) with a lithium fluoride curved crystal 0.5 mm in thickness. The spectra were taken by the CR system with a wide dynamic range, and relative X-ray intensity was calculated from Dicom digital data. Fig. 6 shows measured spectra from the copper target. When the tube voltage was increased, the bremsstrahlung X-ray intensity increased, and the characteristic X-ray intensity of K_α and K_β lines also increased. Following insertion of the copper filter, since the bremsstrahlung X-rays with energies higher than the K-absorption edge were absorbed effectively, we observed the edge.

4. Radiography

The quasi-monochromatic radiography was performed with a tube voltage of 20 kV using the filter. Fig. 7 shows radiography for imaging a polycapillary plate, and the radiograms of the polycapillary are shown in Fig. 8. The center of the black spot in the polycapillary radiogram was mainly imaged by direct transmission beams through capillary holes. As shown in this figure, both the spot density and the dimensions hardly varied according to decreases in the polymethyl methacrylate (PMMA) spacer height.

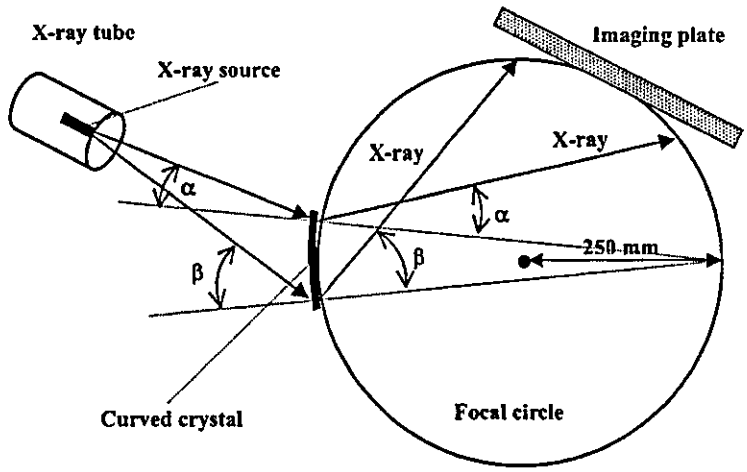

Fig. 5. Transmission-type spectrometer with a lithium fluoride curved crystal and an imaging plate. The X-rays from the source are diffracted by the crystal and are imaged on the imaging plate.

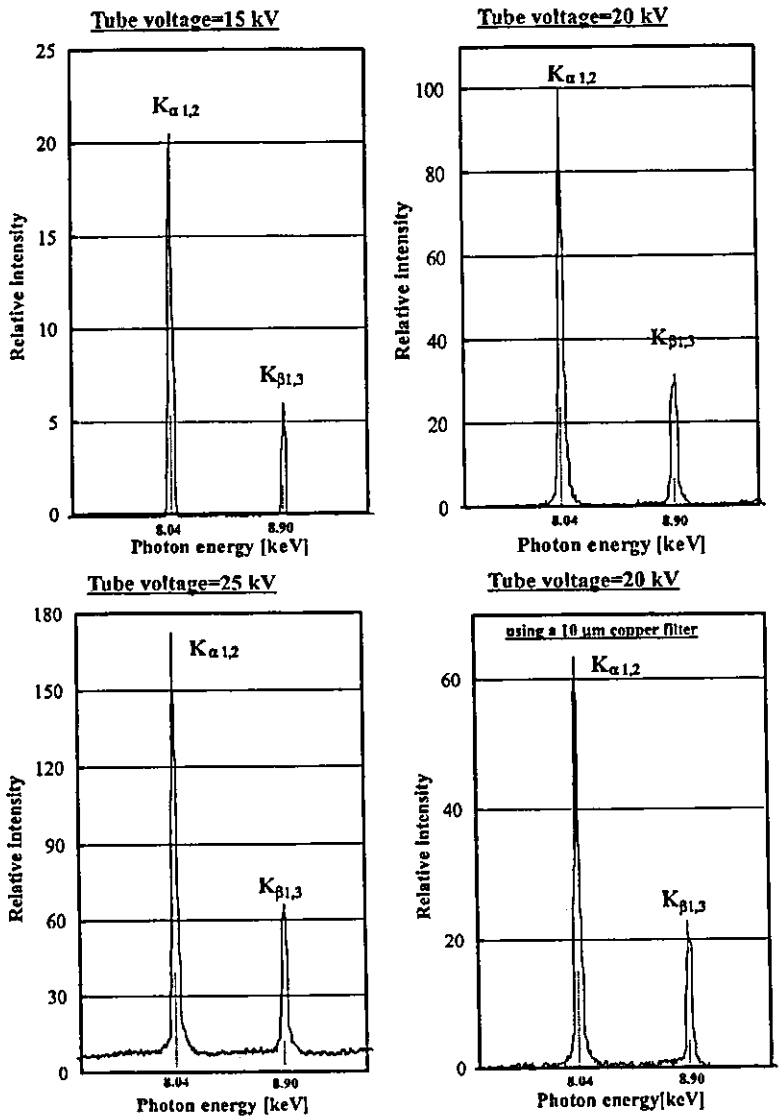

Fig. 6. Measured X-ray spectra according to changes in the tube voltage. Both the bremsstrahlung and characteristic X-ray intensities increased with corresponding increases in the tube voltage, and we determined the conditions for radiography as follows: a tube voltage of 20 kV and a filter thickness of 10 μm.

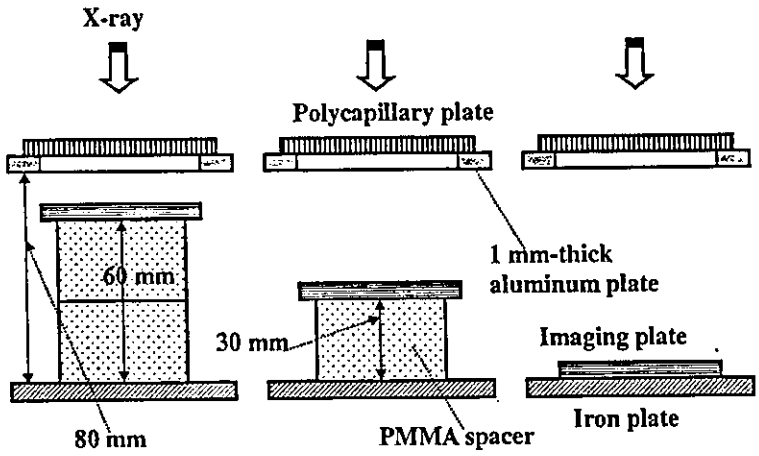

Fig. 7. Radiography for imaging a polycapillary plate according to changes in the distance between the polycapillary and imaging plates. Because the distance was regulated by the spacer thickness, the distance decreased according to increases in the spacer height.

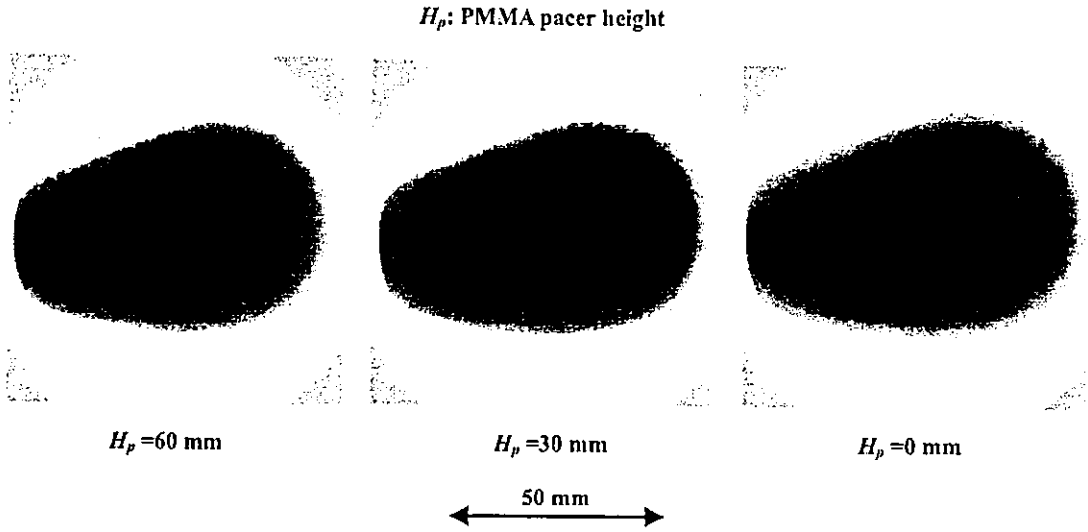

Fig. 8. Radiograms of a polycapillary plate according to changes in the PMMA height.

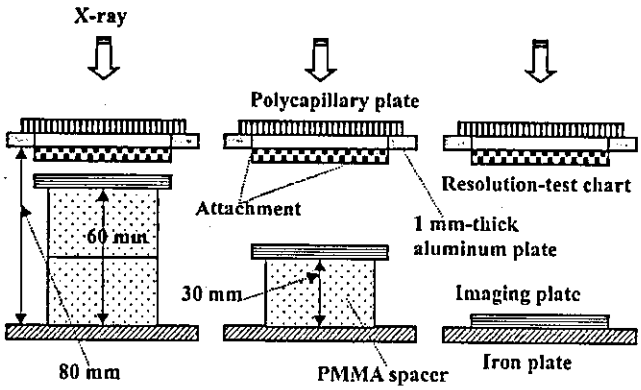

Fig. 9. Radiography for imaging a test chart using a polycapillary plate.

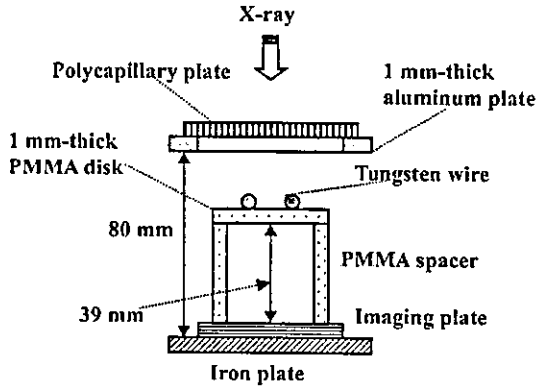

Fig. 11. Radiography for imaging tungsten wires using the polycapillary.

Fig. 9 shows the parallel radiography for imaging a test chart, and the polycapillary was placed on the aluminum plate. In this radiography, when the spacer height was increased, we observed 100 μm lines, and the image dimensions decreased slightly (Fig. 10).

Figs. 11 and 12 show radiography and the radiogram of tungsten wires on a PMMA spacer, respectively. Although the image contrast increased with increases in the wire diameter, a 50 μm-diameter wire could be observed. An angiography of a rabbit heart is shown in Fig. 13; iodine-based

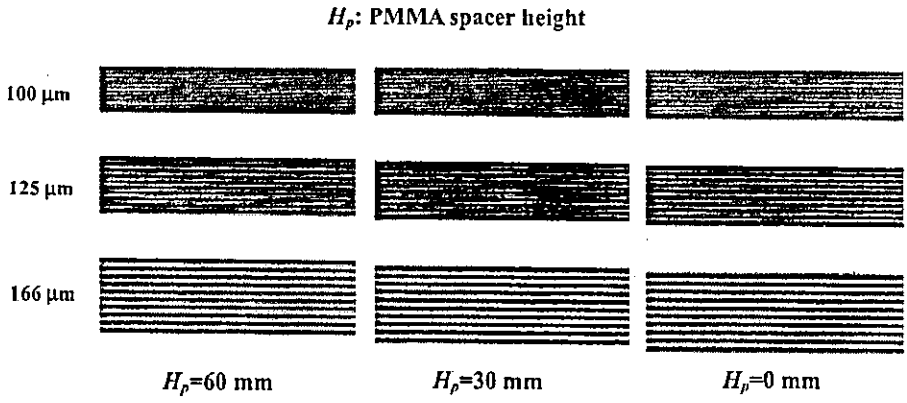

Fig. 10. Radiograms of a test chart using the polycapillary according to changes in the height.

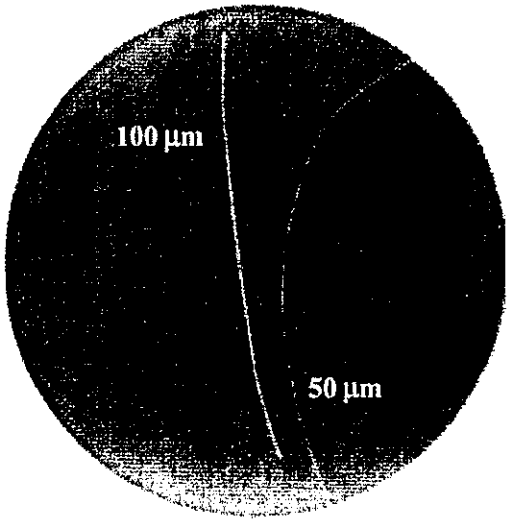

Fig. 12. Radiograms of tungsten wires on a PMMA spacer.

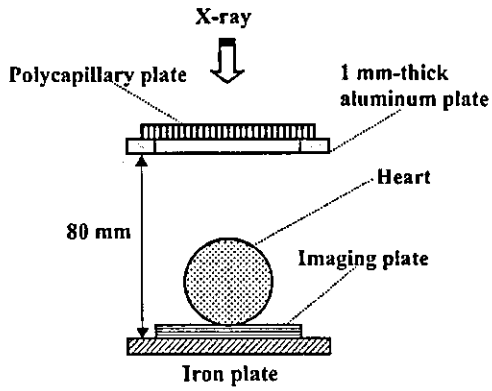

Fig. 13. Parallel angiography of a heart extracted from a rabbit using iodine-based microspheres.

microspheres of 15 μm-diameter were used, and fine blood vessels of about 100 μm were clearly visible (Fig. 14).

5. Discussion

Using this polycapillary plate, we performed a quasi-monochromatic parallel radiography system using a polycapillary plate in conjunction with a CR system.

If we assume that the incident angle for reflection in the capillary hole is constant, the X-ray intensity without absorbing I_0, the transmission intensity I_t, the reflecting intensity I_r, and the intensity for parallel radiography I may be given by (Fig. 15):

$$I_0 = K_1 \sum_{i=1}^{n} I_k(E_i) \exp\{-\mu(E_i)a\}, \quad (1)$$

$$I_t \cong K_2 \sum_{i=1}^{n} I_k(E_i) \exp\{-\mu(E_i)a - \mu_c(E_i)b\}, \quad (2)$$

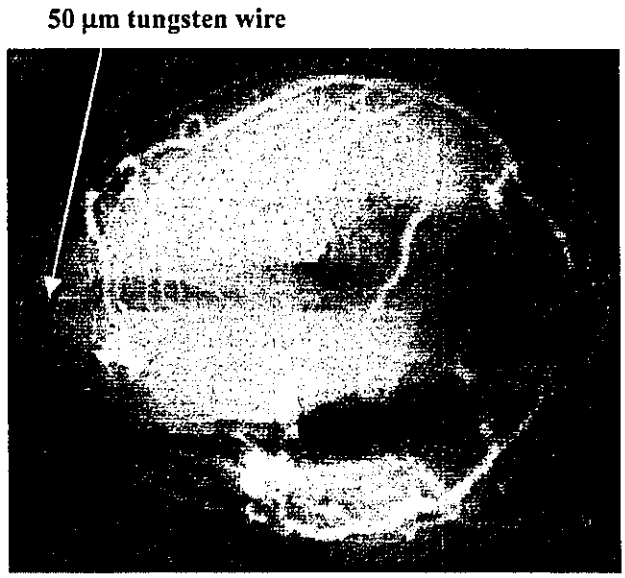

Fig. 14. Angiogram of the heart using the polycapillary.

$$I_r \cong K_3 \sum_{i=1}^{n} I_k(E_i) \exp\{-\mu(E_i)a\} \cdot R(E_i)^m, \quad (3)$$

$$I \cong I_0 + I_r \gg I_t, \quad (4)$$

where $I_k(E_i)$ is the ith characteristic X-ray intensity from the tube, $\mu(E_i)$ the linear absorption coefficient of copper filter, $\mu_c(E_i)$ is the linear absorption coefficient of capillary glass, $R(E_i)$ is the reflecting power ($1 \geqq R(E_i) \geqq 0$), m is the number of reflection, n is the number of characteristic X-rays, a is the filter thickness, b is capillary thickness, and K_1–K_3 are constants.

In this research, we performed parallel radiography achieved with a polycapillary plate in conjunction with quasi-monochromatic X-rays, and higher image resolutions as compared with those obtained without using the plate were obtained. Currently, because the resolution improves

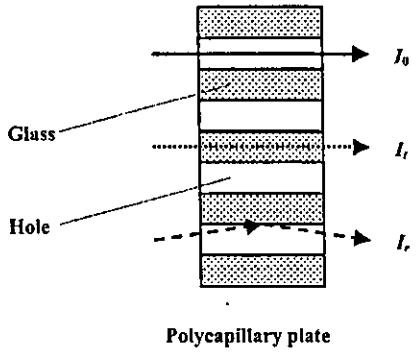

Fig. 15. Characteristic X-ray transmissions in the polycapillary plate. In the parallel radiography, the radiographic object is taken by both the direct transmission rays through capillaries I_0 and the reflection rays on the insides of holes I_r.

with corresponding decreases in the hole diameter of the capillary, this system can be applied to image a wide variety of objects in various fields including medical radiography.

6. Summary

In summary, we developed a conventional quasi-monochromatic parallel radiography system utilizing a polycapillary plate with a hole diameter of 25 μm and a CR system. Quasi-monochromatic characteristic X-rays were obtained by a 10 μm-thick copper filter with a tube voltage of 20 kV. The X-rays from the tube were formed into parallel beams in order to perform radiography. The image dimension increased slightly with corresponding increases in the distance between the radiographic object and the imaging plate, and we observed a 50 μm tungsten wire and fine blood vessels clearly.

Acknowledgements

This work was supported by Grants-in-Aid for Scientific Research and Advanced Medical Scientific Research from MECSST (12670902, 13470154, and 13877114), Grants from Keiryo Research Foundation, JST (Test of Fostering Potential), NEDO, and MHLW (HLSRG, RAMT-nano-001, RHGTEFB-genome-005, and RGCD13C-1).

References

[1] E. Sato, S. Kimura, S. Kawasaki, H. Isobe, K. Takahashi, Y. Tamakawa, T. Yanagisawa, Rev. Sci. Instrum. 61 (1990) 2343.
[2] E. Sato, A. Shikoda, S. Kimura, M. Sagae, T. Oizumi, K. Takahashi, Y. Hayasi, T. Shoji, K. Shishido, Y. Tamakawa, T. Yanagisawa, SPIE 1801 (1992) 628.
[3] E. Sato, M. Sagae, K. Takahashi, T. Oizumi, H. Ojima, K. Takayama, Y. Tamakawa, T. Yanagisawa, A. Fujiwara, K. Mitoya, SPIE 2513 (1994) 649.
[4] E. Sato, M. Sagae, K. Takahashi, A. Shikoda, T. Oizumi, H. Ojima, K. Takayama, Y. Tamakawa, T. Yanagisawa, A. Fujiwara, K. Mitoya, SPIE 2513 (1994) 723.
[5] A. Shikoda, E. Sato, M. Sagae, T. Oizumi, Y. Tamakawa, T. Yanagisawa, Rev. Sci. Instrum. 65 (1994) 850.
[6] E. Sato, K. Takahashi, M. Sagae, S. Kimura, T. Oizumi, Y. Hayasi, Y. Tamakawa, T. Yanagisawa, Med. Biol. Eng. Comput. 32 (1994) 289.
[7] K. Takahashi, E. Sato, M. Sagae, T. Oizumi, Y. Tamakawa, T. Yanagisawa, Jpn. J. Appl. Phys. 33 (1994) 4146.
[8] E. Sato, M. Sagae, A. Shikoda, K. Takahashi, T. Oizumi, M. Yamamoto, A. Takabe, K. Sakamaki, Y. Hayasi, H. Ojima, K. Takayama, Y. Tamakawa, SPIE 2869 (1996) 937.
[9] E. Sato, R. Germer, Y. Hayasi, E. Tanaka, H. Mori, T. Kawai, T. Usuki, K. Sato, H. Obara, M. Zuguchi, T. Ichimaru, H. Ojima, K. Takayama, H. Ido, SPIE 4948 (2002) 604.
[10] E. Sato, Y. Hayasi, R. Germer, E. Tanaka, H. Mori, T. Kawai, H. Obara, T. Ichimaru, K. Takayama, H. Ido, Jpn. J. Med. Imag. Inform. Sci. 20 (2003) 148.
[11] E. Sato, Y. Hayasi, R. Germer, E. Tanaka, H. Mori, T. Kawai, H. Obara, T. Ichimaru, K. Takayama, H. Ido, Jpn. J. Med. Phys. 20 (2003) 123.
[12] H. Mori, K. Hyodo, E. Tanaka, M.U. Mohammed, A. Yamakawa, Y. Shinozaki, H. Nakazawa, Y. Tanaka, T. Sekka, Y. Iwata, S. Honda, K. Umetani, H. Ueki, T. Yokoyama, K. Tanioka, M. Kubota, H. Hosaka, N. Ishizawa, M. Ando, Radiology 201 (1996) 173.
[13] T.J. Davis, D. Gao, T.E. Gureyev, A.W. Stevenson, S.W. Wilkims, Nature 373 (1995) 595.
[14] A. Momose, T. Takeda, Y. Itai, K. Hirano, Nat. Med. 2 (4) (1996) 473.
[15] A. Ishisaka, H. Ohara, C. Honda, Opt. Rev. 7 (2000) 566.
[16] A.A. Bzhanmikov, N. Langhoff, J. Schmalz, R. Wedell, V.L. Beloglazov, N.F. Lebedev, SPIE 3444 (1998) 430.
[17] Q.F. Xiao, S.V. Poturaef, Nucl. Instr. Meth. Phys. Res. A 347 (1994) 376.
[18] E. Sato, Y. Hayasi, E. Tanaka, H. Mori, T. Kawai, H. Obara, T. Ichimaru, K. Takayama, H. Ido, T. Usuki, K. Sato, Y. Tamakawa, SPIE 4508 (2001) 176.
[19] E. Sato, H. Toriyabe, Y. Hayasi, E. Tanaka, H. Mori, T. Kawai, T. Usuki, K. Sato, H. Obara, T. Ichimaru, K. Takayama, H. Ido, Y. Tamakawa, SPIE 4682 (2002) 298.
[20] E. Sato, Y. Hayasi, T. Usuki, K. Sato, H. Ojima, K. Takayama, H. Ido, in: Proceedings of the 3rd Korea-Japan Joint Meeting on Medical Physics, Gyeongju, 2002, p. 400.
[21] E. Sato, K. Sato, Y. Tamakawa, Ann. Rep. Iwate Med. Univ. Sch. Lib. Arts Sci. 35 (2000) 13.

Available online at www.sciencedirect.com
SCIENCE DIRECT®
Journal of Electron Spectroscopy and Related Phenomena 137–140 (2004) 713–720
JOURNAL OF ELECTRON SPECTROSCOPY and Related Phenomena
www.elsevier.com/locate/elspec

Sharp characteristic X-ray irradiation from weakly ionized linear plasma

E. Sato [a,*], Y. Hayasi [a], R. Germer [b], E. Tanaka [c], H. Mori [d], T. Kawai [e], T. Ichimaru [f], S. Sato [g], K. Takayama [h], H. Ido [i]

[a] Department of Physics, Iwate Medical University, Morioka 020-0015, Japan
[b] ITP, FHTW FB1 and TU-Berlin, D 12249 Berlin, Germany
[c] Department of Nutritional Science, Faculty of Applied Bio-science, Tokyo University of Agriculture, Setagayaku 156-8502, Japan
[d] Department of Cardiac Physiology, National Cardiovascular Center Research Institute, Osaka 565-8565, Japan
[e] Electron Tube Division #2, Hamamatsu Photonics Inc., Iwata-gun 438-0193, Japan
[f] Department of Radiological Technology, School of Health Sciences, Hirosaki University, Hirosaki 036-8564, Japan
[g] Department of Microbiology, School of Medicine, Iwate Medical University, Morioka 020-8505, Japan
[h] Shock Wave Research Center, Institute of Fluid Science, Tohoku University, Sendai 980-8577, Japan
[i] Department of Applied Physics and Informatics, Faculty of Engineering, Tohoku Gakuin University, Tagajo 985-8537, Japan

Available online 21 March 2004

Abstract

In the plasma flash X-ray generator, a high-voltage main condenser of approximately 200 nF is charged up to 50 kV by a power supply, and electric charges in the condenser are discharged to an X-ray tube after triggering the cathode electrode. Flash X-rays are then produced. The X-ray tube is a demountable triode connected to a turbo molecular pump with a pressure of approximately 1 mPa. As electrons from the cathode electrode are roughly focused onto a rod nickel target of 3.0 mm in diameter by the electric field in the X-ray tube, a weakly ionized linear plasma consisting of nickel ions and electrons forms by target evaporation. At a charging voltage of 50 kV, the maximum tube voltage was almost equal to the charging voltage of the main condenser, and the peak current was about 17 kA. When the charging voltage was increased, the linear plasma formed, and the intensities of K-series characteristic X-rays increased. The K-series lines were quite sharp and intense, and hardly any bremsstrahlung rays were detected. The X-ray pulse widths were approximately 700 ns, and the time-integrated X-ray intensity had a value of approximately 30 μC/kg at 1.0 m from the X-ray source at a charging voltage of 50 kV.

Keywords: Flash X-ray; Weakly ionized linear plasma; K-series characteristic X-rays; Quasi-monochromatic X-rays; Monochromatic X-rays

1. Introduction

Flash X-ray generators utilizing condensers are of great technological importance due to their extremely short X-ray durations, and several different types of generators have been developed for specific radiographic applications [1,2]. In particular, flash X-ray generators with energies lower than 150 keV have been developed in order to perform soft radiographies with biomedical applications [3–8], and these generators have large capacity condensers in order to increase the X-ray intensity by increasing electrostatic energy.

Using a gas-discharge capillary [9–12], soft X-ray lasers have been produced to form a linear plasma, in which the laser intensity increases proportionally to the capillary length. However, it is quite difficult to increase the laser photon energy beyond 10 keV. Because there are no X-ray resonators in the high photon energy region, new methods for increasing coherence will be desired in the future.

By forming a weakly ionized linear plasma [13–16] using plate and rod targets, we confirmed the production of intense K-series characteristic X-rays along the plasma axial direction. In these experiments, because we employed a transmission-type X-ray spectrometer utilizing an X-ray film, it was difficult to determine the relative intensities of the characteristic X-rays.

In this paper, we describe a flash X-ray generator utilizing a large capacity condenser of 200 nF and a rod-target

* Corresponding author.
E-mail address: dresato@iwate-med.ac.jp (E. Sato).

0368-2048/$ – see front matter © 2004 Elsevier B.V. All rights reserved.
doi:10.1016/j.elspec.2004.02.009

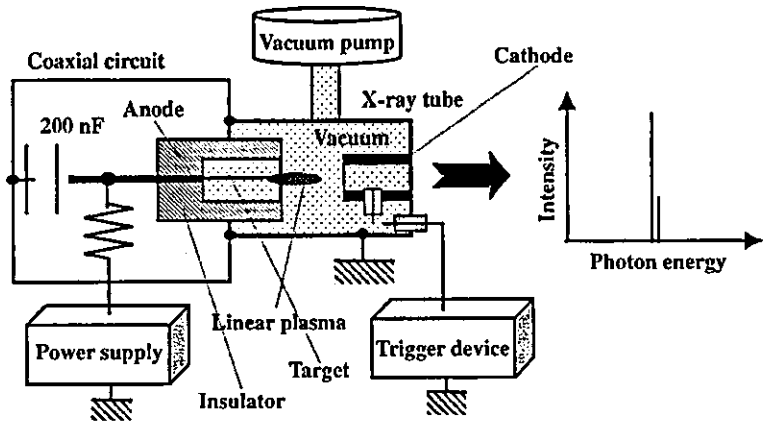

Fig. 1. Block diagram of the high-intensity plasma flash X-ray generator. This generator employs a large capacity condenser in order to increase the characteristic X-ray intensities in a low photon energy region by increasing the electrostatic energy in the condenser.

radiation tube, used to perform a preliminary experiment for generating intense and sharp monochromatic X-rays by forming a linear nickel plasma cloud around a fine target.

2. Generator

2.1. High-voltage circuit

Fig. 1 shows a block diagram of the high-intensity plasma flash X-ray generator. This generator consists of the following essential components: a high-voltage power supply, a high-voltage condenser with a capacity of approximately 200 nF, a turbo-molecular vacuum pump, a krytron pulse generator as a trigger device, and a flash X-ray tube. In this generator, a low-impedance transmission line is employed in order to increase maximum tube current. The high-voltage main condenser is charged to 50 kV by the power supply, and electric charges in the condenser are discharged to the tube after triggering the cathode electrode. The plasma flash X-rays are then produced.

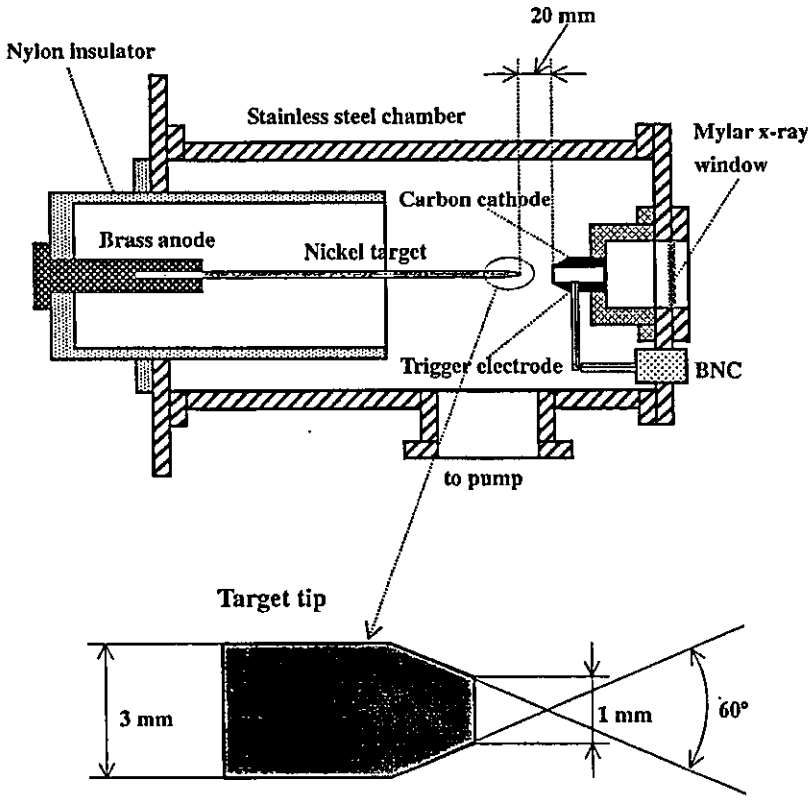

Fig. 2. Schematic drawing of the flash X-ray tube with a rod target. The tube utilizes a long target to form a weakly ionized linear plasma to absorb bremsstrahlung X-rays produced in the plasma, which transmits the characteristic X-rays easily due to the absorption coefficient.

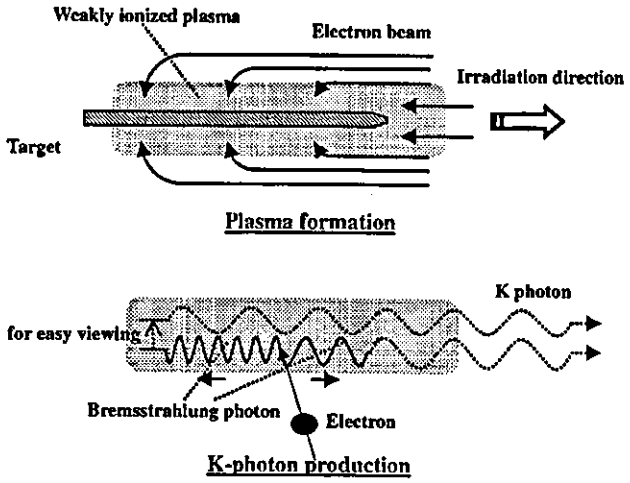

Fig. 3. K-photon irradiation from the plasma. The bremsstrahlung X-rays are absorbed and are converted into fluorescent (characteristic) X-rays in the weakly ionized linear plasma.

2.2. X-ray tube

The X-ray tube is a demountable cold cathode triode connected to a turbo-molecular pump. The pressure in the tube is approximately 1 mPa (Fig. 2). The tube consists of the following major parts: a hollow cylindrical carbon cathode with a bore diameter of 10.0 mm, a trigger electrode made from copper wire, a stainless steel vacuum chamber, a nylon insulator, a polyethylene terephthalate (Mylar) X-ray window 0.25 mm in thickness, and a rod-shaped nickel target 3.0 mm in diameter with a tip angle of 60°. The distance between the target and cathode electrodes is approximately 20 mm, and the trigger electrode is set in the cathode electrode. The electron beam from the cathode electrode is roughly focused onto the target by the electric field in the tube, and evaporation leads to the formation of a weakly ionized linear plasma of nickel ions and electrons around the fine target.

2.3. Principle of characteristic X-ray irradiation

In the linear plasma, bremsstrahlung photons with energies higher than the K-absorption edge are effectively absorbed and are converted into fluorescent X-rays (Fig. 3). The plasma then transmits the fluorescent rays easily, and bremsstrahlung rays with energies lower than the K-edge are also absorbed by the plasma. In addition, because bremsstrahlung rays are not emitted in the direction opposite that of electron acceleration, intense characteristic X-rays are generated along axial direction of the plasma.

3. Characteristics

3.1. Tube voltage and current

The tube voltage and current were measured by a high-voltage divider with an input impedance of 1 GΩ and a current transformer, respectively. Fig. 4 shows the time relation for the tube voltage and current. At the indicated charging voltages, they displayed damped oscillations. When the charging voltage was increased, both the maximum tube voltage and current increased. At a charging voltage of 50 kV, the maximum tube voltage was almost equal to the charging voltage of the main condenser, and the maximum tube current was approximately 17 kA.

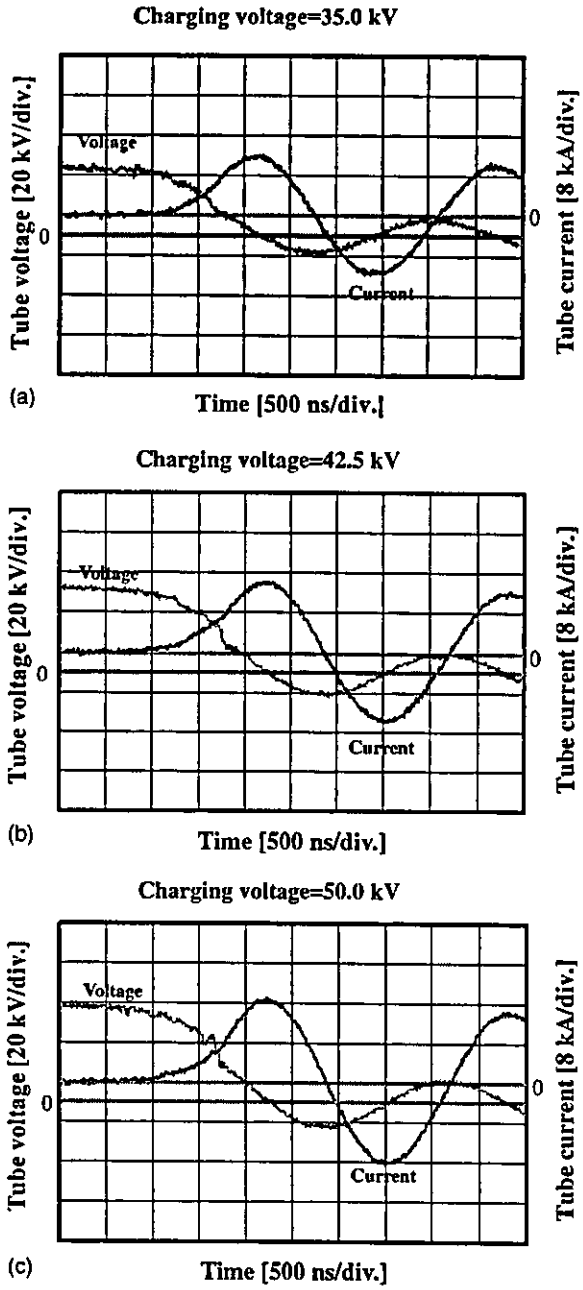

Fig. 4. Tube voltages and currents with a charging voltage of (a) 35.0, (b) 42.5, and (c) 50.0 kV.

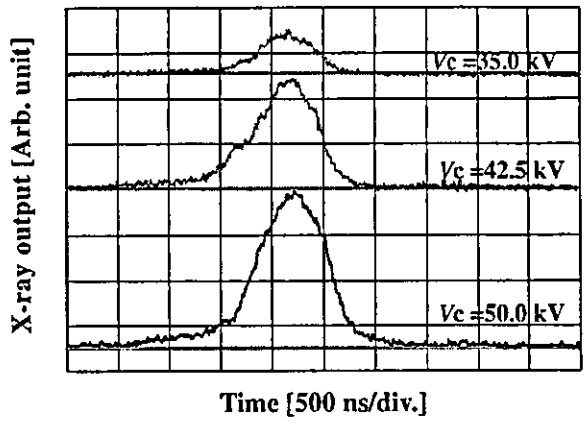

Fig. 5. X-ray outputs measured by a plastic scintillator with changes in the charging voltage.

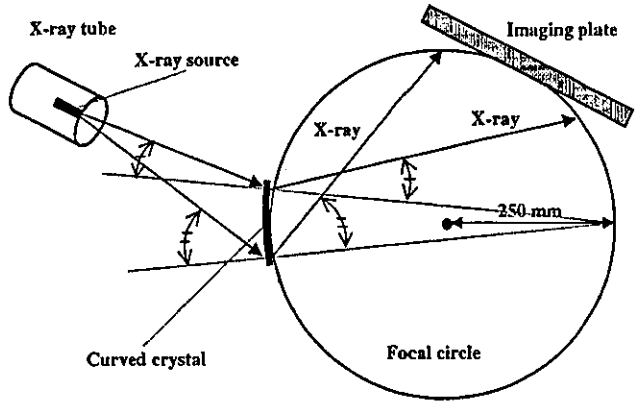

Fig. 7. Transmission-type spectrometer with a lithium fluoride curved crystal and an imaging plate. The X-rays from the source are diffracted by the crystal and are imaged by the imaging plate.

3.2. X-ray output

X-ray output pulse was detected using a combination of a plastic scintillator and a photomultiplier (Fig. 5). The X-ray pulse height substantially increased with corresponding increases in the charging voltage. The X-ray pulse widths were about 700 ns, and the time-integrated X-ray intensity per pulse, measured by a thermoluminescence dosimeter (Kyokko TLD Reader 1500 having MSO-S elements without energy compensation), had a value of about 30 μC/kg at 1.0 m from the X-ray source with a charging voltage of 50 kV.

3.3. X-ray source

The images of the plasma X-ray source were taken using a pinhole camera with a hole diameter of 100 μm (Fig. 6). When the charging voltage was increased, the plasma X-ray source grew, and both the beam dimension and the intensity increased.

3.4. X-ray spectra

X-ray spectra from the plasma source were measured by a transmission-type spectrometer (Fig. 7) with a lithium fluoride curved crystal of 0.5 mm in thickness. The spectra were taken by a computed radiography (CR) system (Konica Regius 150) [17] with a wide dynamic range, and the relative X-ray intensity was calculated from Dicom digital data. Fig. 8 shows measured spectra from the nickel target. We observed quite sharp lines of K-series characteristic X-rays such as lasers, while bremsstrahlung rays were hardly detected. The characteristic X-ray intensities of K_α and K_β lines substantially increased with corresponding increases in the charging voltage, and the K_β line was absorbed by a monochromatic cobalt filter of 15 μm thickness.

3.5. X-ray divergence

In order to ascertain the difference in characteristics between X-rays from a conventional tube and these from the

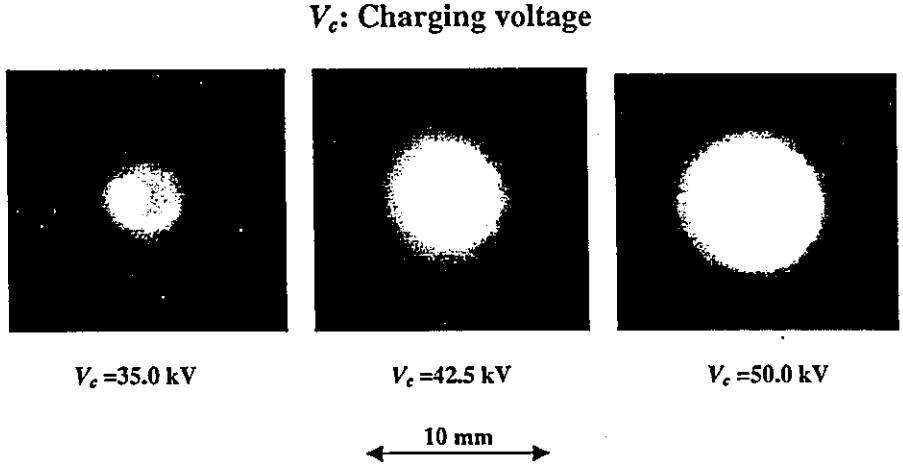

Fig. 6. Images of the plasma X-ray source measured by a pinhole of 100 μm from the plasma axial direction.

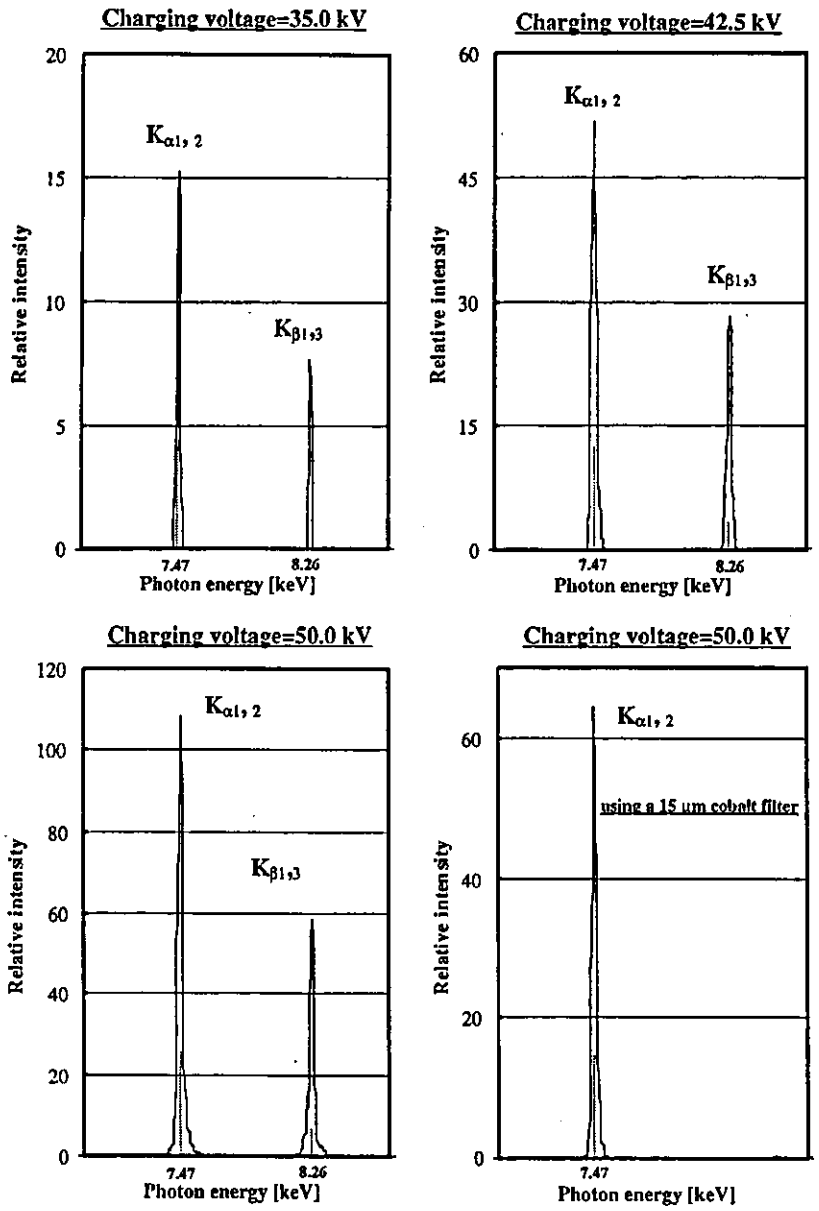

Fig. 8. X-ray spectra from weakly ionized nickel plasma according to changes in the charging voltage and to insertion of a cobalt monochromatic filter. In the measurement, we observed very sharp and intense characteristic X-rays such as lasers, while bremsstrahlung X-rays were hardly detected at all.

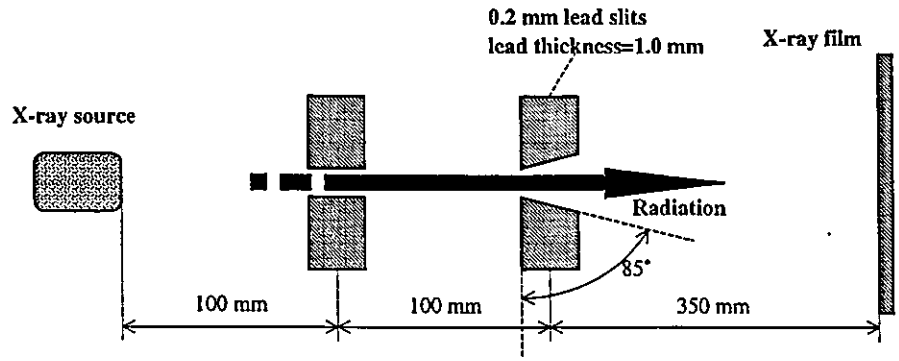

Fig. 9. Experimental setup for measuring X-ray divergence using two lead slits.

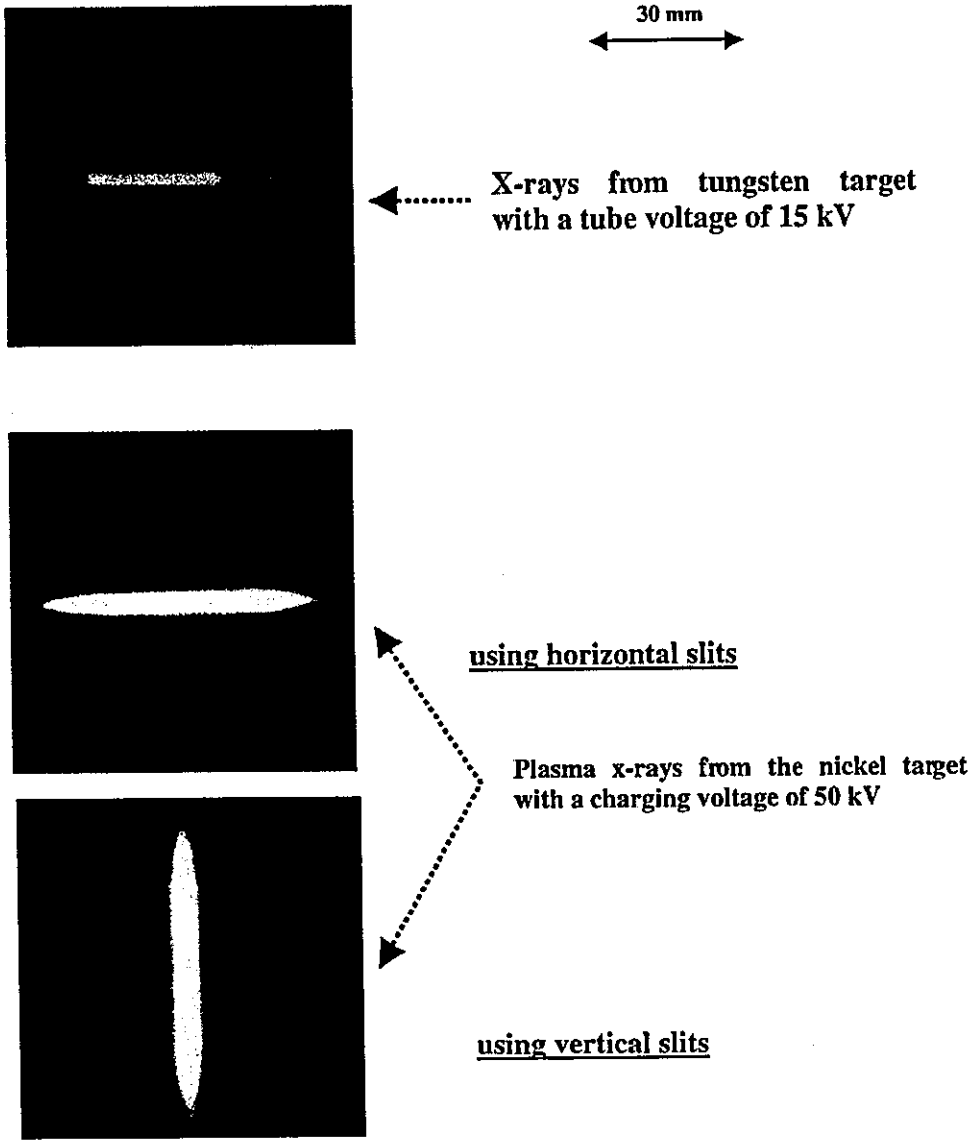

Fig. 10. X-ray divergence with two lead slits. The characteristic X-rays from the plasma were diffused greatly after passing through two lead slits.

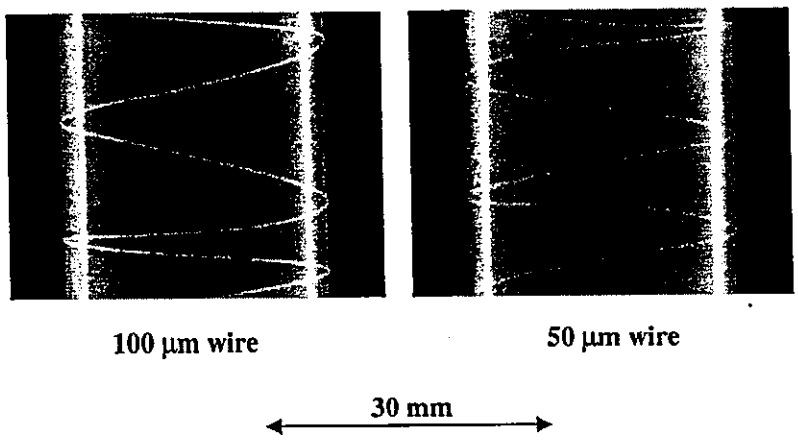

Fig. 11. Radiograms of tungsten wires of 50 and 100 μm in diameter coiled around pipes made of polymethyl methacrylate.

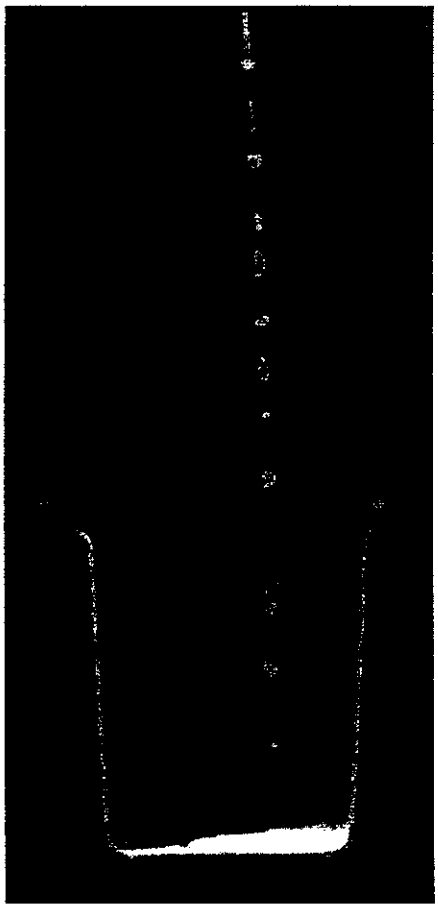

Fig. 12. Radiogram of water droplets falling into a polypropylene beaker from an injector.

plasma tube, we employed two lead slits in order to measure the divergence of the X-rays (Fig. 9). As compared with X-rays from a conventional tube with a tungsten target, the characteristic X-rays from the linear plasma were diffused greatly after passing through the two slits (Fig. 10).

4. Radiography

The plasma radiography was performed by the CR system (Konica Regius 150) without using a monochromatic filter, and the distance between the X-ray source and imaging plate was 1.2 m.

Firstly, the image resolution was measured using wires. Fig. 11 shows radiograms of tungsten wires coiled around pipes made of polymethyl methacrylate at a charging voltage of 50 kV. Although the image contrast increased with increases in the wire diameter, a 50 μm-diameter wire could be observed.

The image of water droplets falling into a polypropylene beaker from an injector is shown in Fig. 12. This image

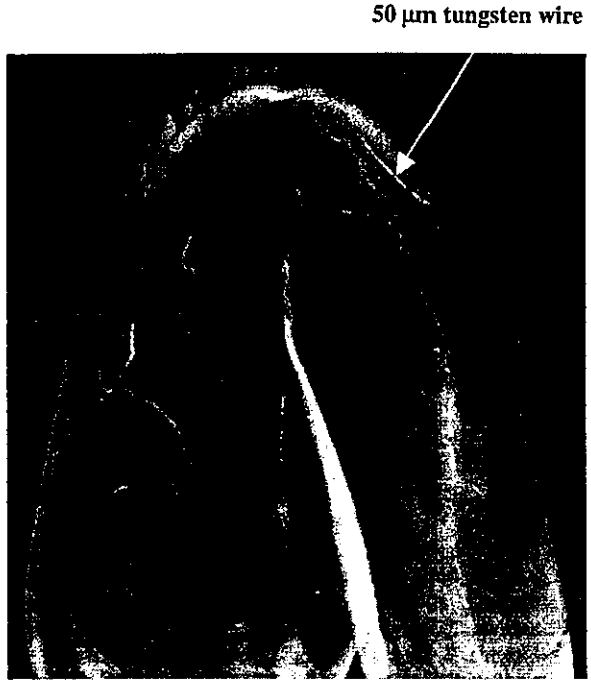

Fig. 13. Angiograms of the external ear of a rabbit.

was taken at a charging voltage of 45 kV, with the slight addition of an iodine-based contrast medium. Because the X-ray duration was about 1 μs, the stop-motion image of water could be obtained.

Fig. 13 shows an angiogram of the external ear of a rabbit; iodine-based microspheres of 15 μm diameter were used at a charging voltage of 45 kV, and fine blood vessels of about 50 μm were clearly visible.

5. Discussion

Regarding the spectrum measurement, although we obtained quite intense and sharp K-series lines without bremsstrahlung X-rays by forming a linear plasma X-ray source, we could not observe the difference between the $K\alpha_1$ and $K\alpha_2$ lines. In addition, we confirmed the divergence of K-series characteristic X-rays using two lead slits, and the maximum divergence angle was approximately 0.5°.

If we assume that the characteristic and bremsstrahlung X-rays are signal and noise, respectively, the signal to noise ratio is higher than 1000:1, and this value is almost equal to those of soft X-ray lasers produced by the gas-discharge capillary.

In this research, we obtained sufficient characteristic X-ray intensity per pulse for CR radiography, and the generator produced number of characteristic photons of approximately 1×10^{14} photons/cm^2 s at 1.0 m from the source. In addition, since the photon energy of characteristic X-rays can be controlled by changing target elements, various quasi-monochromatic high-speed radiographies,

such as high-contrast micro angiography[22] and parallel radiography[23] using an X-ray lens, will be possible.

Acknowledgements

This work was supported by Grants-in-Aid for Scientific Research and Advanced Medical Scientific Research from MECSST (12670902, 13470154, and 13877114), Grants from Keiryo Research Foundation, JST (Test of Fostering Potential), NEDO, and MHLW (HLSRG, RAMT-nano-001, RHGTEFB-genome-005, and RGCD13C-1).

References

[1] A. Mattsson, Physica Scripta 5 (1972) 99.
[2] R. Germer, J. Phys. E: Sci. Instrum. 12 (1979) 336.
[3] E. Sato, H. Isobe, F. Hoshino, Rev. Sci. Instrum 57 (1986) 1399.
[4] E. Sato, S. Kimura, S. Kawasaki, H. Isobe, K. Takahashi, Y. Tamakawa, T. Yanagisawa, Rev. Sci. Instrum. 61 (1990) 2343.
[5] A. Shikoda, E. Sato, M. Sagae, T. Oizumi, Y. Tamakawa, T. Yanagisawa, Rev. Sci. Instrum. 65 (1994) 850.
[6] E. Sato, K. Takahashi, M. Sagae, S. Kimura, T. Oizumi, Y. Hayasi, Y. Tamakawa, T. Yanagisawa, Med. Biol. Eng. Comput. 32 (1994) 289.
[7] K. Takahashi, E. Sato, M. Sagae, T. Oizumi, Y. Tamakawa, T. Yanagisawa, Jpn. J. Appl. Phys. 33 (1994) 4146.
[8] E. Sato, M. Sagae, A. Shikoda, K. Takahashi, T. Oizumi, M. Yamamoto, A. Takabe, K. Sakamaki, Y. Hayasi, H. Ojima, K. Takayama, Y. Tamakawa, SPIE 2869 (1996) 937.
[9] J.J. Rocca, V. Shlyaptsev, F.G. Tomasel, Phys. Rev. Lett. 73 (1994) 2192.
[10] G.P. Collins, Phys. Today 10 (1994) 19.
[11] J.J.G. Rocca, J.L.A. Chilla, S. Sakadzic, SPIE 4505 (2001) 1.
[12] S. Le Pape, P. Zeitoun, J.J.G. Rocca, SPIE 4505 (2001) 23.
[13] E. Sato, Y. Suzuki, Y. Hayasi, E. Tanaka, H. Mori, T. Kawai, K. Takayama, H. Ido, Y. Tamakawa, SPIE 4505 (2001) 154.
[14] E. Sato, Y. Hayashi, E. Tanaka, H. Mori, T. Kawai, H. Obara, T. Ichimaru, K. Takayama, H. Ido, T. Usuki, K. Sato, Y. Tamakawa, SPIE 4508 (2001) 176.
[15] E. Sato, Y. Hayasi, R. Germer, E. Tanaka, H. Mori, T. Kawai, H. Obara, T. Ichimaru, K. Takayama, H. Ido, Jpn. J. Med. Imag. Inform. Sci. 20 (2003) 148.
[16] E. Sato, Y. Hayasi, R. Germer, E. Tanaka, H. Mori, T. Kawai, H. Obara, T. Ichimaru, K. Takayama, H. Ido, Jpn. J. Med. Phys. 20 (2003) 123.
[17] E. Sato, K. Sato, Y. Tamakawa, Ann. Rep. Iwate Med. Univ. Sch. Lib. Arts Sci. 35 (2000) 13.

In Situ Measurements of Crossbridge Dynamics and Lattice Spacing in Rat Hearts by X-Ray Diffraction

Sensitivity to Regional Ischemia

James T. Pearson, PhD; Mikiyasu Shirai, MD, PhD; Haruo Ito, PhD; Noriyuki Tokunaga, MD; Hirotsugu Tsuchimochi, PhD; Naoki Nishiura; Daryl O. Schwenke, PhD; Hatsue Ishibashi-Ueda, MD; Ryuichi Akiyama, PhD; Hidezo Mori, MD, PhD; Kenji Kangawa, PhD; Hiroyuki Suga, MD, PhD; Naoto Yagi, PhD

Background—Synchrotron radiation has been used to analyze crossbridge dynamics in isolated papillary muscle and excised perfused hearts with the use of x-ray diffraction techniques. We showed that these techniques can detect regional changes in rat left ventricle contractility and myosin lattice spacing in in situ ejecting hearts in real time. Furthermore, we examined the sensitivity of these indexes to regional ischemia.

Methods and Results—The left ventricular free wall of spontaneously beating rat hearts (heart rate, 290 to 404 bpm) was directly exposed to brief high-flux, low-emittance x-ray beams provided at SPring-8. Myosin mass transfer to actin filaments was determined as the decrease in reflection intensity ratio (intensity of 1,0 plane over the 1,1 plane) between end-diastole and end-systole. The distance between 1,0 reflections was converted to a lattice spacing between myosin filaments. We found that mass transfer (mean, 1.71±0.09 SEM, n=13 hearts) preceded significant increases in lattice spacing (2 to 5 nm) during systole in nonischemic pericardium. Left coronary occlusion eliminated increases in lattice spacing and severely reduced mass transfer ($P<0.01$) in the ischemic region.

Conclusions—Our results suggest that x-ray diffraction techniques permit real-time in situ analysis of regional crossbridge dynamics at molecular and fiber levels that might also facilitate investigations of ventricular output regulation by the Frank-Starling mechanism. **(*Circulation*. 2004;109:2976-2979.)**

Key Words: ischemia ■ myocardial contraction ■ myosin ■ radiography

Despite the history of studies on crossbridge dynamics, lower photon counts and poorer quality of diffraction patterns obtained from cardiac muscle than skeletal and insect flight muscles[1–3] have limited progress with cardiac muscle until recently.[4,5] Some of us used third-generation synchrotron radiation (SPring-8, Japan Synchrotron Radiation Research Institute) to determine x-ray diffraction patterns in excised, perfused rat hearts while moving systematically across the left ventricular (LV) equator from the epicardium through to the ventricular cavity.[6]

X-ray diffraction patterns of cardiac muscle produce 2 equatorial-position reflections from the lattice-like arrangement of its protein elements.[2] Mass transfer of myosin heads to actin during contraction is inferred from a decrease in the integrated 1,0 reflection intensity ($I_{1,0}$, lattice plane containing only thick myosin filaments) and an increase in 1,1 reflection intensity ($I_{1,1}$, plane with thick myosin and thin actin filaments).[7] The myocardial intensity ratio (defined as $I_{1,0}/I_{1,1}$) is minimal in the rigor state and maximal in a quiescent state.[1,2,6,8]

Furthermore, the distance between 1,0 reflection peaks ($d_{1,0}$ spacing) represents the myosin lattice spacing, which is inversely related to sarcomere length in isolated fibers[5] as static myocytes maintain a constant cell volume. Whether decreases in myofilament spacing contribute to increasing Ca^{2+} sensitivity and increased probability of crossbridge formation at longer sarcomere lengths has been actively debated.[9] However, it is still not known if lattice spacing is regulated to maintain constant lattice volume (ie, if lattice cross-sectional area decreases with increasing sarcomere length, then interfilament spacing must decrease) during dynamic contractions in vivo.

Recently, it was shown that the intensity ratio derived from x-ray diffraction patterns of isolated whole hearts decreased during isovolumic contractions with a similar time course throughout the LV,[6] implying that crossbridge cycling in fibers of different myocardial layers is similar despite differences in fiber orientation and rate of short-

Received March 1, 2004; de novo received March 31, 2004; revision received May 6, 2004; accepted May 6, 2004

From the National Cardiovascular Center Research Institute, Osaka, Japan (J.T.P., M.S., N.T., H.T., N.N., D.O.S., H.I-U., H.M., K.K., H.S.); S-I Medico-Tech Co Ltd, Kashiwara, Osaka, Japan (H.I.); Muroran Institute of Technology, Muroran, Japan (R.A.); and SPring-8/JASRI, Sayo, Hyogo, Japan (N.Y.)

Correspondence to Dr James T. Pearson, Cardiac Physiology, National Cardiovascular Center Research Institute, 5-7-1 Fujishirodai, Suita, Osaka 565-8565 Japan. E-mail jpearson@ri.ncvc.go.jp

Circulation is available at http://www.circulationaha.org

DOI: 10.1161/01.CIR.0000133322.19340.EF

ening. However, it was not possible to follow dynamic lattice spacing changes. In the present study, we used a fine-focused x-ray beam to record diffraction patterns of a localized region of the LV of ejecting rat hearts in situ and then determined crossbridge cycling and myosin lattice spacing.

Methods

Animals and Surgical Preparation

Anesthetized (50 mg/kg sodium pentobarbital IP) male Sprague-Dawley rats (Japan SLC, Hamamatsu, Japan), 9 to 10 weeks of age (350 to 400 g), were artificially ventilated and thoracotomized. Procedures were performed according to SPring-8 guidelines for the care and welfare of experimental animals. The heart was continuously irrigated while the apex was raised by a manipulator paddle and restrained by 2 superficial sutures in the LV to minimize vertical movements. Pressure-volume loops were recorded from an apically inserted 1.4F micromanometer (SPR-671 Millar Instruments) and a 1.5F conductance catheter (S-1 Medico-tech Co Ltd, Osaka)[10] to determine the temporal sequence of cardiac events and heart rate (determined from end-diastole [ED] interval).

X-Ray Diffraction With Collimated Synchrotron Radiation

Measurements were conducted at the 40XU beamline of SPring-8.[6] A collimated quasimonochromatic beam (wavelength, 0.08 nm) with a beam flux of ~10^{12} photons per second (15 keV; ring current, 60 to 100 mA) and dimensions 0.2 × 0.2 mm was focused at an oblique tangent to the myocardium (~3 m from the detector). The ventilator was stopped at end-expiration to reduce heart movements during measurements (~2.1 seconds). Images were digitally recorded at a 15-ms sampling interval with the use of an image intensifier and a fast CCD camera,[6] simultaneous with pressure-volume analog signals (1000-Hz sampling frequency). The beam passed through the apical myocardium between the ends of the descending branch of the left coronary artery (LAD) and the posterior interventricular vein. Final burning of the recorded region (higher energy levels) confirmed that the beam only exposed fibers in the epicardium and part of the intermediate layer (histological inspection).

Acute Ischemia Treatment

Heart baseline recordings were established, permanent ligation of the proximal LAD was performed, and recordings were repeated 5 to 10 minutes later.

Intensity Ratio Calculations and Analyses

Integrated intensity of $I_{1,0}$ and $I_{1,1}$ was determined from the areas under the reflection peaks after background subtraction.[6] Intensity ratio ($I_{1,0}/I_{1,1}$) was used rather than absolute reflection intensities of $I_{1,0}$ and $I_{1,1}$, which are influenced by changes in the quantity of fibers sampled during contractions.[3] Myosin mass transfer index was defined as the difference in intensity ratio between ED and end systole (ES).

Results

Mass Transfer and Lattice Spacing in Nonischemic Hearts

Intensity ratio significantly decreased during systole (increase in LV pressure [LVP] and decrease in LV volume [LVV]) and conversely, increased during diastole under the baseline rhythm (Figure 1a). Averaging intensity ratio over multiple beats reduced variability during diastole in the otherwise sinusoidal patterns (black lines, Figure 1b). With regard to time, $d_{1,0}$ spacing increased continuously

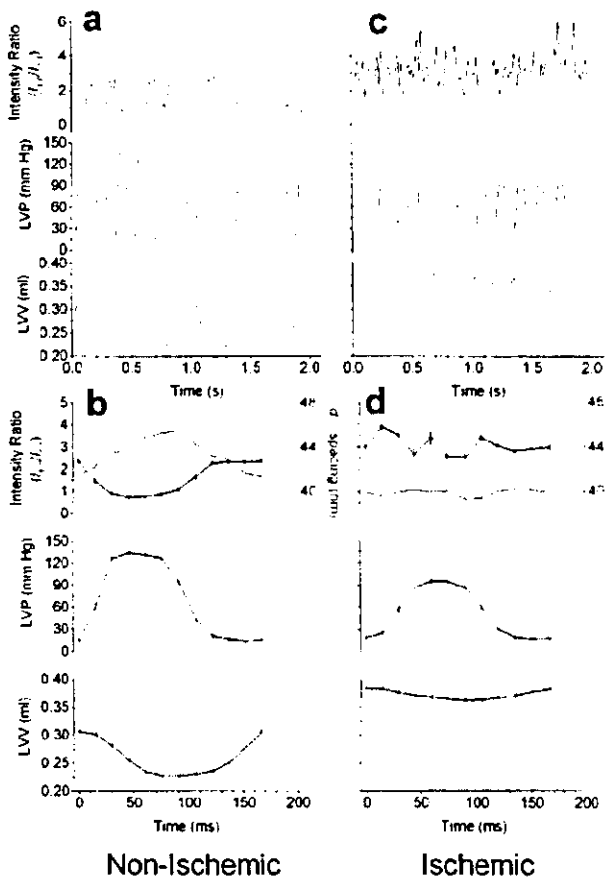

Figure 1. Relations between calculated intensity ratio, $d_{1,0}$ spacing, LVP, and LVV obtained from an LV with the use of x-ray diffraction. a and c, Consecutive records (15-ms intervals) of intensity ratio, LVP, and LVV during the baseline (a) and after LAD occlusion (c) in the same heart. b and d, Average changes in intensity ratio (black lines), $d_{1,0}$ spacing (red lines), LVP, and LVV over the cardiac cycle between the ED events (derived from a and c, respectively; bars indicate SEM).

during systole and then decreased during diastole, suggesting that considerable changes occur in the myofilament spacing (red line, Figure 1b).

Intensity ratio averaged 2.80±0.11 (SEM, n=13 hearts) at ED, and the average myosin mass transfer index was 1.71±0.09. In all hearts, the decrease in intensity ratio during crossbridge formation was completed before the full extent of the $d_{1,0}$ spacing change (2 to 5 nm between hearts, Figure 2a). Furthermore, at any given LVV, the $d_{1,0}$ spacing during systole was 1 to 2 nm larger than diastole (Figure 2b).

Mass Transfer and Lattice Spacing During Regional Ischemia

LAD occlusion reduced the intensity ratio change and prevented normal lattice spacing increase, consistent with reduced contractility of the ischemic region (Figure 1, c and d). Occlusion significantly increased intensity ratios at both ED ($P<0.05$) and ES ($P<0.001$) in the same LV region (n=6,

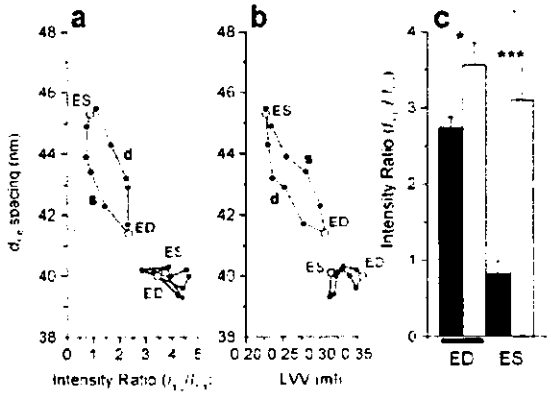

Figure 2. a and b, Average loops formed between $d_{1,0}$ spacing, LVV, and intensity ratio during consecutive cycles (shown in Figure 1) under baseline conditions (black symbols) and regional ischemia (red symbols). Systolic (s) and diastolic (d) trajectories are indicated for baseline. c, Mean intensity ratio at ED and ES during baseline (black columns) and regional ischemia (open columns; group mean ± SEM). Ischemia versus baseline, paired *t* test **P*<0.05, ****P*<0.001.

Figure 2c). Although mean heart rate was not depressed (341±16 bpm, 4% increase) and there was only a small decrease in mean LV ES pressure (−26.9±5.8 mm Hg SEM), regional ischemia severely depressed the mass transfer index (55% of baseline).

Discussion

Our data clearly demonstrate that current synchrotron technology can produce sufficient energy to obtain well-defined reflections from single exposures to enable calculation of intensity ratio and $d_{1,0}$ spacing in in situ rat hearts (Figure 1). The mean ED intensity ratio of this study is similar to 2.96 obtained from LV in arrested rat hearts under normoxic perfusion.[5] Furthermore, in rat papillary muscles, the resting ratio was 3.07.[1,2] The results presented here were restricted to epicardial recordings (within 0.8-mm depth), consisting of helically orientated fibers, to minimize the contributions from fibers with orientations that vary at greater depth.[11] Nevertheless, it was recently established that neither diastolic intensity ratio nor mass transfer varies with depth of x-ray beam penetration in beating, perfused hearts (paced at 2 Hz).[6]

In Situ Changes in Myofilament Spacing

We showed that significant lattice expansion occurs during contraction and that the relation between $d_{1,0}$ spacing and intensity ratio is not linear but a loop in nonischemic hearts (black line, Figure 2a). The $d_{1,0}$ spacing changes during contraction (2 to 5 nm) were larger than the 1-nm difference in $d_{1,0}$ spacing reported between the epicardium and endocardium (at diastole).[6] Therefore, the larger $d_{1,0}$ spacing change found in ejecting hearts cannot be explained by shifts in the fiber layers exposed to the beam. The loop formed by these indexes might contain valuable information about how crossbridge axial and radial forces alter the dynamics of lattice spacing changes. Crossbridge projections from the myosin backbone produce radial force perpendicular to that of axial force in the filament direction.[12] Release of isometric tension in intact skeletal myofibers during sarcomere shortening causes a brief and rapid lattice spacing increase, in excess of that predicted by fiber shortening in itself.[12,13] We therefore conclude that lattice volume is not constant in the dynamic state because myosin lattice spacing is significantly larger (1 to 2 nm) during contraction than ventricular filling at the same LVV ($d_{1,0}$ spacing during systole greater than diastole, Figure 2b). Crossbridge formation probably causes a brief lattice expansion in ejecting hearts mediated by radial forces.

Sensitivity of In Situ Indexes to Regional Ischemia

The relevance of our new findings is that although the intensity ratio of beating hearts in diastole was similar to that of relaxed papillary muscles, there is a very different response of the myocardium in beating hearts to ischemia in terms of crossbridge dynamics and lattice space changes. Higher intensity ratios and more variable intensity ratio changes during systole (Figure 1, c and d) occurred as the result of lower absolute $I_{1,1}$ in systole and a lack of consistent increase in $I_{1,1}$ when $I_{1,0}$ decreased (data not shown). Thus, permanent regional ischemia severely attenuated mass transfer in the epicardium (Figure 2c). Furthermore, ischemia induced increases in ED intensity ratio in vivo, whereas other studies report maximal decreases in the intensity ratio under anoxic perfusion (isolated arrested hearts)[5] or rigor.[1,2] An increase in intensity ratio might be related to metabolite accumulation or pronounced passive stretching, because fiber shortening in infarcted regions progressively decreases until fibers eventually become passively stretched (bulging) by fiber shortening in the nonischemic region.[14] In support of the bulging possibility, we found that $d_{1,0}$ spacing no longer increases between ED and ES after occlusion.

The cellular basis of the Frank-Starling law of the heart involves increases in contractility caused by length-dependent increases in Ca^{2+} sensitivity associated with increased ventricular filling.[9] However, it is still debated whether increased crossbridge activation results from increased probability of crossbridge formation with decreasing lattice spacing associated with fiber stretching (see review in Reference 9). In a future publication, we will examine how LV volume loading influences mass transfer in relation to myofilament spacing and length-dependent activation of contraction in situ.

Acknowledgments

This work was supported by the Promotion of Fundamental Studies in Health Sciences of the Organization for Pharmaceutical Safety and Research (OPSR) and Ministerial grants Nano-001 and a Grant-in-Aid for Scientific Research. The experiments were made with approval of the SPring-8 Program Review Committee. We thank Dr Keiji Umetani for access to the Medical Imaging Center.

References

1. Matsubara I, Kamiyama A, Suga H. X-ray diffraction study of contracting heart muscle. *J Mol Biol*. 1977;111:121–128.
2. Matsubara I, Suga H, Yagi N. An X-ray diffraction study of the cross-circulated canine heart. *J Physiol (London)*. 1977;270:311–320.

3. Yagi N, Saeki Y, Ishikawa T, et al. Cross-bridge and calcium behavior in ferret papillary muscle in different thyroid states. *Jpn J Physiol*. 2001;51:319–326.
4. Konhilas JP, Irving TC, de Tombe PP. Myofilament calcium sensitivity in skinned rat cardiac trabeculae: role of interfilament spacing. *Circ Res*. 2002;90:59–65.
5. Irving TC, Konhilas J, Perry D, et al. Myofilament lattice spacing as a function of sarcomere length in isolated rat myocardium. *Am J Physiol*. 2000;279:H2568–H2573.
6. Yagi N, Shimizu J, Mohri S, et al. X-ray diffraction from a left ventricular wall of rat heart. *Biophys J*. 2004;86:2286–2294.
7. Huxley HE, Brown W. The low-angle x-ray diagram of vertebrate striated muscle and its behaviour during contraction and rigor. *J Mol Biol*. 1967;30:383–434.
8. Sowerby AJ, Harries J, Diakun GP, et al. X-ray diffraction studies of whole rat heart during anoxic perfusion. *Biochem Biophys Res Commun*. 1994;202:1244–1251.
9. Konhilas JP, Irving TC, de Tombe PP. Frank-Starling law of the heart and the cellular mechanisms of length-dependent activation. *Pflugers Arch*. 2002;445:305–310.
10. Ito H, Takaki M, Yamaguchi H, et al. Left ventricular volumetric conductance catheter for rats. *Am J Physiol*. 1996;270:H1509–H1514.
11. Streeter DD Jr, Spotnitz HM, Patel DP, et al. Fiber orientation in the canine left ventricle during diastole and systole. *Circ Res*. 1969;24:339–347.
12. Cecchi G, Bagni MA, Griffiths PJ, et al. Detection of radial cross-bridge force by lattice spacing changes in intact single muscle fibers. *Science*. 1990;250:1409–1411.
13. Bagni M, Cecchi G, Griffiths P, et al. Lattice spacing changes accompanying isometric tension development in intact single muscle fibers. *Biophys J*. 1994;67:1965–1975.
14. Lew WYW, Chen Z, Guth B, et al. Mechanisms of augmented segment shortening in nonischemic areas during acute ischemia of the canine left ventricle. *Circ Res*. 1985;56:351–358.

ELSEVIER

Cardiovascular Research 64 (2004) 125–131

Cardiovascular Research

www.elsevier.com/locate/cardiores

Extraneuronal enzymatic degradation of myocardial interstitial norepinephrine in the ischemic region

Takafumi Fujii[a], Toji Yamazaki[a,*], Tsuyoshi Akiyama[a], Shunji Sano[b], Hidezo Mori[a]

[a] *Department of Cardiac Physiology, National Cardiovascular Center Research Institute, 5-7-1 Fujishiro-dai, Suita, Osaka 565-8565, Japan*
[b] *Department of Cardiovascular Surgery, Okayama University Medical School, Okayama 700-8558, Japan*

Received 19 March 2004; received in revised form 28 May 2004; accepted 14 June 2004
Available online 22 July 2004
Time for primary review 26 days

Abstract

Objective: Catechol *O*-methyltransferase (COMT) is believed to exert degradative action at high norepinephrine (NE) levels. Although COMT exists in cardiac tissues, the contribution of cardiac COMT activity to regional NE kinetics, particularly in ischemia-induced NE accumulation, remains unclear. We investigated the role of cardiac COMT in NE kinetics in the ischemic region. **Methods:** We implanted a microdialysis probe into the left ventricular myocardium of anesthetized rabbits and induced myocardial ischemia by 60-min coronary artery occlusion. We monitored myocardial interstitial levels of NE and its metabolites in the presence and absence of a COMT inhibitor. We intraperitoneally administered entacapone (10 mg/kg) 120 min before control sampling. **Results:** In control, entacapone increased interstitial dihydroxyphenylglycol (DHPG, intraneuronal NE metabolite by monoamine oxidase (MAO)) levels and decreased interstitial normetanephrine (NMN, extraneuronal NE metabolite by COMT) and 3-methoxy-4-hydroxyphenylglycol (MHPG, extraneuronal DHPG metabolite by COMT) levels, but did not change interstitial NE levels. Coronary occlusion increased NE levels to 165 ± 48 nM at 45–60 min of occlusion. This increase was accompanied by increases in DHPG and NMN levels (11.3 ± 1.1 and 9.3 ± 1.3 nM at 45–60 min of occlusion). Entacapone augmented the ischemia-induced NE and DHPG responses (333 ± 51 and 22.9 ± 2.4 nM at 45–60 min of occlusion). In contrast, the ischemia-induced NMN response was suppressed by entacapone (2.0 ± 0.4 nM at 45–60 min of occlusion). Reperfusion decreased interstitial NE levels and increased interstitial DHPG and NMN levels. Entacapone suppressed changes in NE and NMN levels, but augmented the increase in dialysate DHPG. **Conclusion:** Myocardial ischemia evoked increases in myocardial interstitial NE and NMN levels. COMT inhibition augmented the increase in NE (substrate of COMT) levels and suppressed the increase in NMN (metabolite by COMT) levels. In the ischemic heart, COMT contributes to the removal of accumulated NE in the myocardium.

Keywords: Adrenergic agonists; Autonomic nervous system; Ischemia; Reperfusion; Neurotransmitters

1. Introduction

It has been reported that myocardial ischemia evokes an excessive norepinephrine (NE) accumulation in the myocardial interstitial space [1,2]. Outward NE transport through the uptake$_1$ carrier has been proposed as an important mechanism responsible for this ischemia-induced NE accumulation [2–4]. The presence of such high NE levels in the myocardial interstitium may be involved in the progression of myocardial cell injury and a higher incidence of malignant arrhythmia [5,6].

In the non-ischemic heart, released NE is reclaimed by cardiac sympathetic nerve endings via the uptake$_1$ carrier and repackaged or metabolized to dihydroxyphenylglycol (DHPG) by monoamine oxidase (MAO). NE, which escapes the synapses to the myocardial interstitium, spills over into the bloodstream or is taken up by extraneuronal cells via the uptake$_2$ carrier and mainly degraded to NE metabolites by catechol *O*-methyltransferase (COMT) [6–9] (Fig. 1). In the ischemic heart, normal transport by the uptake$_1$ carrier is impaired and NE spills over into the bloodstream, which is decreased due to the reduction of myocardial blood flow [1]. Therefore, extraneuronal enzymatic degradation may be the only mechanism that decreases myocardial interstitial NE. Little information, however, is available on the extraneuronal NE degradation by COMT in the ischemic region [10,11].

* Corresponding author. Tel.: +81-6-6833-5012x2380; fax: +81-6-6872-8092.
E-mail address: yamazaki@ri.ncvc.go.jp (T. Yamazaki).

0008-6363/$ - see front matter © 2004 European Society of Cardiology. Published by Elsevier B.V. All rights reserved.
doi:10.1016/j.cardiores.2004.06.011